

Gravitational wave source populations: Disentangling an AGN component

V. GAYATHRI,^{1,2} DANIEL WYSOCKI,² Y. YANG,¹ R. O'SHAUGHNESSY,³ Z. HAIMAN,⁴ H. TAGAWA,⁴ AND I. BARTOS¹

¹*Department of Physics, University of Florida, PO Box 118440, Gainesville, FL 32611-8440, USA*

²*Leonard E. Parker Center for Gravitation, Cosmology, and Astrophysics, University of Wisconsin–Milwaukee, Milwaukee, WI 53201, USA**

³*Center for Computational Relativity and Gravitation, Rochester Institute of Technology, Rochester, NY 14623, USA*

⁴*Department of Astronomy, Columbia University, 550 W. 120th St., New York, NY, 10027, USA*

ABSTRACT

The astrophysical origin of the over 90 compact binary mergers discovered by the LIGO and Virgo gravitational wave observatories is an open question. While the unusual mass and spin of some of the discovered objects constrain progenitor scenarios, the observed mergers are consistent with multiple interpretations. A promising approach to solve this question is to consider the observed distributions of binary properties and compare them to expectations from different origin scenarios. Here we describe a new hierarchical population analysis framework to assess the relative contribution of different formation channels simultaneously. For this study we considered binary formation in AGN disks along with phenomenological models, but the same framework can be extended to other models. We find that high-mass and high-mass-ratio binaries appear more likely to have an AGN origin compared to the same origin as lower-mass events. Future observations of high-mass black hole mergers could further disentangle the AGN component from other channels.

1. INTRODUCTION

Understanding the origin of binary black hole mergers is the first step in utilizing black hole mergers to probe a range of astrophysical processes. The LIGO (Aasi et al. 2015) and Virgo (Acernese et al. 2015) gravitational wave observatories have discovered about 90 binary mergers so far (Abbott et al. 2021a), providing important information on the astrophysical population of mergers. Binary black hole systems can form through various channels, including isolated stellar binaries (Portegies Zwart & Yungelson 1998; Belczynski et al. 2002; Marchant et al. 2016; de Mink & Mandel 2016) or triples (Antonini et al. 2014; Kimpson et al. 2016; Veske et al. 2020), dynamical interactions in star clusters (Sigurdsson & Hernquist 1993; Portegies Zwart & McMillan 2000), primordial black holes formed in the early universe (Carr & Hawking 1974), and in the accretion disks of active galactic nuclei (AGNs; McKernan et al. 2012; Bartos et al. 2017; Stone et al. 2017; Tagawa et al. 2020b; McKernan et al. 2020, 2022).

The increased number of binary black hole observations allows for a more detailed investigation of the population's mass and spin distributions. While individual events may provide anecdotal suggestions hinting at

one formation channel or another, only an interpretation of the full census can enable one to disentangle the potential contributions from multiple formation scenarios. Several studies have previously explored how to disentangle multiple channels, largely relying on comparison to phenomenologically-motivated estimates of the detailed outcomes of full formation scenarios (Doctor et al. 2020; Gerosa & Fishbach 2021; Gayathri et al. 2021, 2020; Yang et al. 2020b; Tagawa et al. 2021; Kimball et al. 2021). Some studies also shown a mixture of channels is strongly preferred over any single channel dominating the detected population (Zevin et al. 2021).

The latest population analysis carried out by LIGO–Virgo–KAGRA, GWTC3 (Abbott et al. 2021a,b), identified several population features that may be indicative of the binaries' origin. First, there appears to be a peak in the binary black hole mass spectrum around 30–40 M_{\odot} compared to a more simple power-law type population (Tiwari & Fairhurst 2021; Talbot & Thrane 2018; Edelman et al. 2022; Sadiq et al. 2022; Fishbach & Holz 2017). At the same time a few observed black holes had unusual properties, such as masses in the so-called upper mass gap ($\gtrsim 50 M_{\odot}$), highly unequal masses in the binary, high spin and precessing mergers, which are rare in stellar evolution and might be indicative of alternative formation scenarios.

* gayathri.v@ligo.org

Here we introduce a flexible approach to compare the predictions of detailed formation models with observations while simultaneously accounting for the potentially-confounding contributions from a flexible phenomenologically-parameterized model for compact binary formation.

Our paper is organised as follows. In section 2 we introduce binary formation in AGN disks, phenomenological descriptions for formation in non-AGN sources, and our flexible parametric population inference method. In section 3, we talk about the analysis’s key findings. In section 4, we summarize our findings and comment on future directions.

2. METHODS

2.1. Binary mergers in AGN disks

We construct a one-parameter model for BBH formation and merger within an AGN disk, parameterized by the maximum mass m_{\max} of the natal BH distribution. Specifically, we adopt a seed BH mass distribution which follows the Salpeter mass function with index 2.35, $dN/dm \propto m^{-2.35}$ with given m_{\max} . For neutron stars (NS) we assume a normal distribution $m/M_{\odot} \sim N(1.49, 0.19)$. The BHs and NSs are assumed to orbit a supermassive black hole in an AGN, migrating into the disk and inward from their natal locations. Close to the AGN, these objects undergo multiple encounters, facilitating binary formation and merger. Other AGN parameters are fiducial values that are expected to be typical, while there are large uncertainties. The range of possible values in the AGN models parameter space is discussed in (McKernan et al. 2018).

Following (Bartos et al. 2017), we adopted a geometrically thin, optically thick, radioactively efficient, steady-state accretion disk expected in AGNs. We used a viscosity parameter $\alpha = 0.1$, radioactive efficiency $\epsilon = 0.1$, fiducial supermassive BH mass $M_{\bullet} = 10^6 M_{\odot}$ and accretion rate $0.1\dot{M}_{\text{Edd}}$, where \dot{M}_{Edd} is the Eddington accretion rate. Using Yang et al. (2020) and Tagawa et al. (2020b,a), we have computed the expected mass and spin distributions of binary mergers in AGNs.

Figure 1 shows the binary black hole merger intrinsic parameter distribution for the AGN model with different initial mass limits ($m_{\max} = [15M_{\odot}, 35M_{\odot}, 50M_{\odot}, 75M_{\odot}]$). As the natal BH mass upper limit m_{\max} increases, more massive binary components and total masses are allowed. At the same time, for high m_{\max} , asymmetric systems are more frequent. By contrast, we have observed that the spin distribution properties are largely independent of our choice for m_{\max} limit.

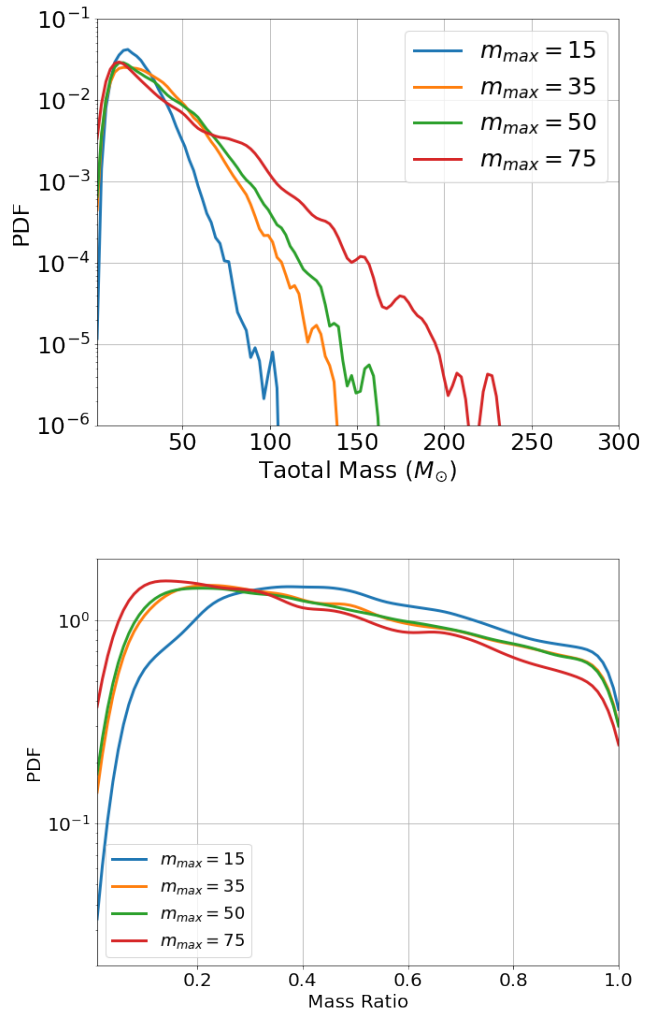


Figure 1. Parameter distributions for binary black holes formed in our AGN disk formation models; line color indicates the maximum natal BH mass. As expected, as the maximum mass increases, total (M) mass upper limits increase. Additionally, a higher BH maximum natal mass m_{\max} increases the relative frequency of asymmetric mergers, particularly highly asymmetric mergers with $q < 1/10$.

2.2. Phenomenology of AGN and non-AGN sources

To allow for binary black holes which have a non-AGN origin, we follow previous work and introduce a few-parameter mixture model family. As illustrated in Figure 2, for the non-AGN component, we allow binary black holes to arise from a mixture of a power law and Gaussian components, as detailed in Table 11 of Abbott et al. (2020). In the power law component, the primary is drawn from a pure power law mass distribution (with some unknown $m_{\max,pl} < 50M_{\odot}$ and unknown primary power law index); the mass ratio is drawn from another power law; and the spins are drawn from an

unknown Beta distribution. In the Gaussian component, the primary and secondary are drawn from two independent Gaussian distributions with unknown mean and variance, with both means confined a priori to be near $30 - 40M_\odot$ to be consistent with expectations for PISN supernovae. By including a second component this phenomenological model can allow for non-power-law features and also allow for spin distributions that vary with mass. Each component k has some undetermined overall rate \mathcal{R}_k . The top panel of Figure 2 shows the general non-AGN model.

Our overall model is therefore a mixture model, parameterized by the unknown (continuous) AGN merger rate and its (discrete) maximum mass m_{\max} , along with all parameters of the non-AGN mixture model. The overall merger rate density $dN/dVdXdT$ can therefore be expressed as a sum

$$\frac{dN}{dVdXdT} = \mathcal{R}_{\text{agn}}p_{\text{agn}}(X|m_{\max}) + \mathcal{R}_g p_g(X|\Lambda_g) + \mathcal{R}_{pl} p_{pl}(X|\Lambda_{pl})$$

where X are binary parameters and where p_q, Λ_q are the model distributions and parameters for the q th component (AGN, Gaussian, and power-law respectively).

To systematically assess how well the distinctive features in AGN formation scenarios can be disentangled from this large model family, we will perform a sequence of calculations with increasing model complexity, as shown in the panels of Figure 2. Specifically, we consider without any non-AGN component; the power-law and Gaussian (PL+G) model only; the power-law and AGN model (PL+AGN), without any Gaussian component; and finally the most general model with all three components.

2.3. Population inference

We describe and demonstrate a flexible parametric method to infer the event rate as a function of compact binary parameters, accounting for Poisson error and selection biases. In (Abbott et al. 2021c), analysed the Multi-Spin model which is the joint mass-spin model for binary black holes. Independent analyses have shown that there is a feature in the BBH mass spectrum around $30-40 M_\odot$, which is modeled as a Gaussian peak on top of a power law continuum. It is an empirical way of modeling extra features, but here we tried to understand it feature with AGN models.

In this section we review the population inference Wysocki et al. (2019) used for multi-formation channel contributions. Binaries with intrinsic parameters x would merge at a rate $dN/dV_c dtdx = \mathcal{R}p(x)$, where N is the number of detections, V_c is the comoving volume, \mathcal{R} is the space-time-independent rate of binary coalescence per unit comoving volume and $p(x)$ is the probabil-

ity of x from detected binaries. The binaries intrinsic parameters includes mass m_i and spins \mathbf{S}_i , where $i = 1, 2$. The likelihood of the astrophysical BBH population at a

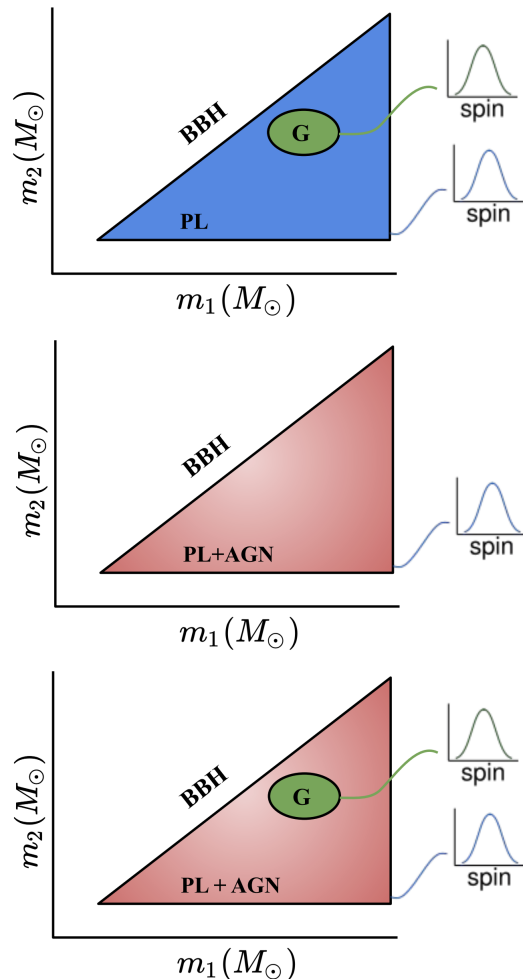


Figure 2. Graphical representations of the BBH population analysis in $m_1 - m_2$ -spin parameter. Top panel for the PL+G, the middle panel for the PL+AGN and the bottom panel for the PL+G+AGN model.

given merger rate \mathcal{R} (Loredo 2004; Mandel et al. 2019; Thrane & Talbot 2019) and given binary intrinsic parameters $X \equiv (m_1, m_2, \chi_1, \chi_2)$, where $\chi_i = \mathbf{S}_i/m_i^2$, given the data for N detections $\mathcal{D} = (d_1, \dots, d_N)$. This the likelihood is given by

$$\mathcal{L}(\mathcal{R}, X) \equiv p(\mathcal{D}|\mathcal{R}, X), \quad (1)$$

$$\mathcal{L}(\mathcal{R}, X) \propto e^{-\mu(\mathcal{R}, X)} \prod_{n=1}^N \int dx \ell_n(x) \mathcal{R} p(x, X), \quad (2)$$

where $\mu(\mathcal{R}, X)$ is the expected number of detections under a given population parametrization X . Using Bayes'

theorem one may obtain a posterior distribution on \mathcal{R} and X after assuming some prior $p(\mathcal{R}, X)$. For computational efficiency and to enable direct comparison with discrete formation models, we use the Gaussian likelihood approximation technique introduced in (Delfavero et al. 2022) to characterize each BBH observation's likelihood $\ell_n(x)$.

Using this formalism, we estimate what fraction of binary black holes are generated via the AGN channel using detected gravitational wave merger information. To do this study we have upgraded current parametric methods with a mixture model feature. Here we have a freedom to do the analysis with number of models which has different astrophysical binary distributions.

3. ANALYSIS

As we discussed before, we perform population inference analysis with mixture model feature and detected confident detection binary black hole detection. For this study we have considered different the astrophysical binary distributions from AGN (with different m_{max}), power-law, Gaussian peak and its combinations (see Figure 2).

3.1. Astrophysical merger rate

We have estimated the astrophysical black hole merger rate for a given astrophysical model with a given number of GW detection. For this study, we have used the parameter estimation samples from obtained by LIGO-Virgo-KAGRA Collaboration (Abbott et al. 2021d,e, 2019, 2021f) and it available in the Gravitational Wave Open Science Center (<https://www.gwopenscience.org>) with the mixed model. Here we follow the same selection criteria as (Abbott et al. (2021b)), we have considered events with a false alarm rate of $< 0.25yr^{-1}$.

Table 1 shows the merger rates inferred for joint PL only, G only, AGN only (with different m_{max}), PL+AGN model (with different m_{max}) and PL+G+AGN models (with different m_{max}). We have estimated the merger rate results derived using each individual model component as well as combined. We have observed that the inferred merger rate from the AGN-only models with different choices for m_{max} produces largely consistent results peaking near $50 Gpc^{-3}yr^{-1}$. For the smallest maximum BH natal mass $m_{max} = 15M_{\odot}$, the inferred single-component AGN merger rate peaks around $80 Gpc^{-3}yr^{-1}$. For all other models, they peak around the same \mathcal{R} . Similarly, we have inferred the merger rate distribution for the single-component Gaussian, and power-law components. As expected, the merger rate from the power-law component dominates

overall, as it incorporates and describes many frequent mergers of the lowest-mass binary black holes. In the case of PL+AGN, the inferred AGN and PL components have a well-determined merger rate, with median AGN merger rate $\simeq 8/, Gpc^{-3}yr^{-1}$ and PL merger rate $\simeq 30/, Gpc^{-3}yr^{-1}$. Changing the maximum natal BH mass m_{max} has a very mild impact on the inferred AGN merger rate, and almost no effect on the inferred PL merger rate.

In the case of PL+G+AGN analyses, the inferred AGN, G and PL components have a well-determined merger rate, with median AGN merger rate $\simeq 7/, Gpc^{-3}yr^{-1}$, G merger rate $\simeq 4/, Gpc^{-3}yr^{-1}$ and PL merger rate $\simeq 30/, Gpc^{-3}yr^{-1}$. As we have seen in the PL+AGN study, we have not seen any major effect on PL or G merger rate when we change the AGN model. Our inferred merger rates deduced from the multi-component model are consistent with inferences performed using single-component models alone, suggesting that inference isolates only the contribution from each component.

3.2. Inferred merger rate versus mass

To better appreciate how well our inference directly projects out the relative contribution from each component, Figure 3.2 and 3.2 shows our inferred merger rate versus mass for PL+AGN and PL+G+AGN models analyses respectively. In each plot we have shown each model component in mass space.

As we expected the low mass region is highly contributed by the PL model compared to other models. We have observed a peak in PL model distribution around $7M_{\odot}$ for both PL+AGN as well as PL+G+AGN analyses. The peak is prominent for the PL+G+AGN study compared to PL+AGN. The high mass region is represented by only AGN, as we expected to see. Note that, the AGN model not only contributes in high mass region it also contributes full mass space as shown in 3.2 and 3.2.

3.3. Inferred merger rate versus mass ratio

Similarly here we show the inferred merger rate versus mass ratio for PL+AGN and PL+G+AGN models analyses.

Figure 3.2 and 3.2 shows our inferred merger rate versus mass ratio for PL+AGN and PL+G+AGN models analyses respectively. In each plot we have shown each model component in mass ratio space. As we expected the low mass ratio region contributed by AGN model for PL+AGN analysis and AGN & G models for PL+G+AGN analysis. For high q , the dominate contribution from PL model, that is consistence with detected events.

Analysis	models	$m_{max} = 15$	$m_{max} = 35$	$m_{max} = 50$	$m_{max} = 75$
PL only		71.9 ^{+19.9} _{-20.4}	-	-	-
G only		19.1 ^{+2.5} _{-2.3}	-	-	-
AGN only		84.7 ^{+19.5} _{-18.5}	49.8 ^{+6.1} _{-5.5}	52.9 ^{+7.8} _{-6.1}	53.2 ^{+7.7} _{-6.2}
PL+AGN	PL	29.3 ^{+9.9} _{-7.2}	28.8 ^{+11.3} _{-6.8}	25.7 ^{+7.6} _{-6.3}	26.8 ^{+9.5} _{-6.2}
	AGN	8.7 ^{+6.3} _{-4.5}	8.3 ^{+8.3} _{-3.7}	12.7 ^{+6.5} _{-4.1}	11.9 ^{+4.6} _{-3.2}
PL+AGN+G	PL	21.3 ^{+7.3} _{-5.2}	23.5 ^{+6.6} _{-5.5}	21.6 ^{+6.7} _{-5.0}	23.3 ^{+7.1} _{-5.0}
	AGN	6.7 ^{+5.6} _{-4.0}	6.2 ^{+5.0} _{-3.5}	12.7 ^{+5.0} _{-4.9}	12.9 ^{+4.3} _{-4.3}
	G	10.2 ^{+2.2} _{-2.3}	9.3 ^{+2.6} _{-3.7}	5.9 ^{+2.9} _{-1.9}	5.6 ^{+2.2} _{-1.5}

Table 1. The astrophysical rates from PL+AGN and PL+AGN+G models. Each row corresponds to each analysis and each column corresponds to different AGN models with different initial mass limit.

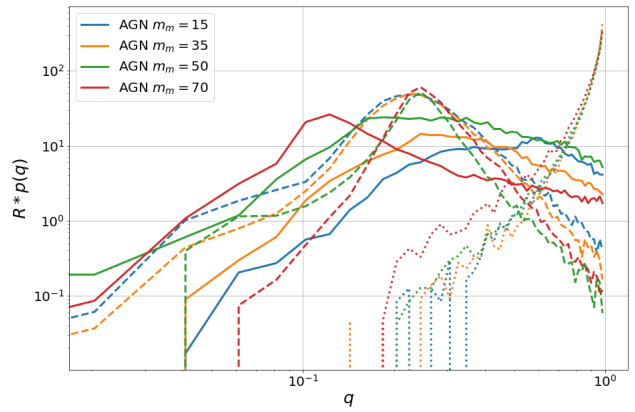
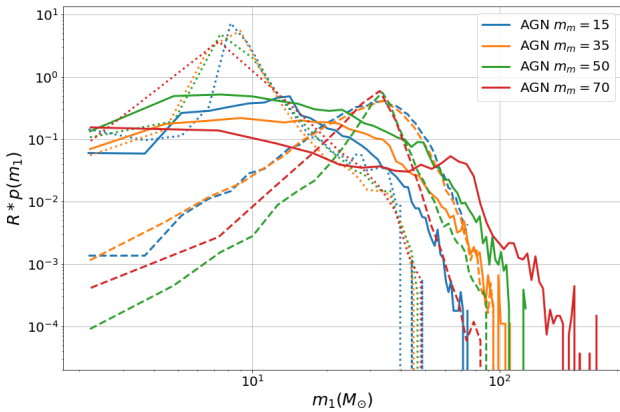
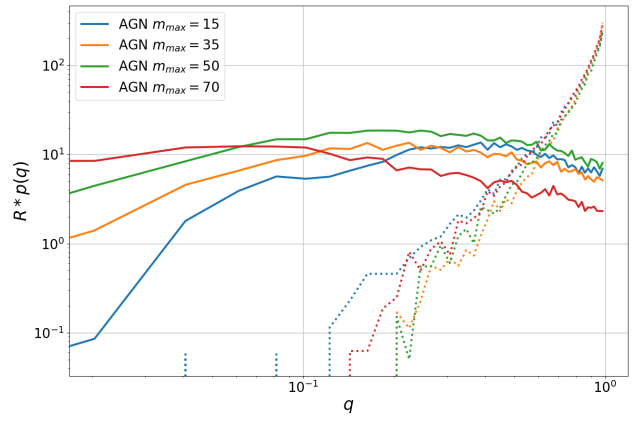
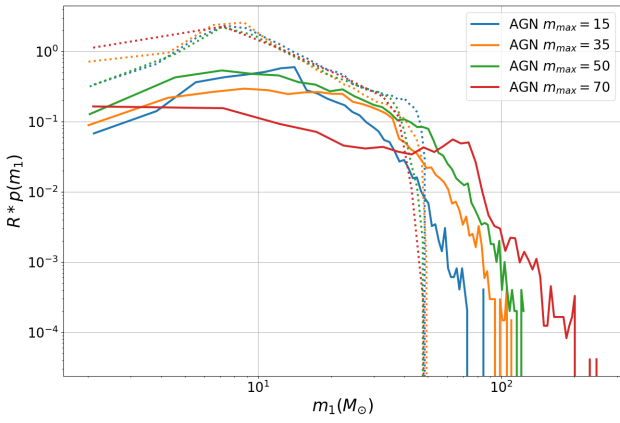


Figure 3. The inferred merger rate versus mass for PL+G+AGN and PL+G+AGN model analyses. The solid, dashed and dotted lines for AGN, G and PL models components.

Figure 4. The inferred merger rate versus mass ratio for PL+AGN and PL+G+AGN model analyses. The solid, dashed and dotted lines for AGN, G and PL models components.

3.4. Power-law model parameters

As we discussed before, the contribution of a power-law model to the overall merger rate does not change substantially if we include or omit other model com-

ponents like AGN or G. Among the models we consider, this quasi-universality is expected: the PL model most effectively reproduces the merger rate versus mass for the lowest-mass and most frequently merging binary

black holes. While the overall merger rate from this component is stable to our choice of the mixture, the model parameters recovered for PL depend strongly on which other confounding contributions are also present, as suggested by Figure 3.2 and 3.2. While the PL mass ratio distribution does not depend strongly on including or omitting AGN or G, the power law slope α and minimum mass m_{min} do change substantially. The estimated α median value with 65% credible intervals from different analysis as $1.6^{+0.2}_{-0.2}$, $6.7^{+3.1}_{-2.4}$, $8.4^{+2.3}_{-3.4}$, and $1.8^{+0.5}_{-0.5}$ for PL-only, PL+G, PL+AGN ($m_{min}=50$) and PL+G+AGN ($m_{min}=50$) respectively. Similarly, m_{min} estimation are $2.5^{+0.3}_{-0.3}$, $8.4^{+0.2}_{-0.3}$, $8.5^{+0.2}_{-0.4}$, and $6.7^{+1.6}_{-1.3}$ for PL-only, PL+G, PL+AGN ($m_{min}=50$) and PL+G+AGN ($m_{min}=50$) respectively. For example, the α estimation suggests that while a pure power-law model favours m_{min} close to the lower limit our priors allow, incorporating other components causes the power-law component's minimum mass to favour larger masses. With the pertinent mass range for the power-law changing substantially via different m_{min} , unsurprisingly. The α estimation has a wide range of inferred power law exponents, as the PL may dominate only an extremely narrow range of masses; see Figure 3.2.

4. CONCLUSION

In this paper, we have directly compared a one-parameter model for AGN binary black hole formation with the reconstructed sample of binary black holes identified via gravitational wave observations. To deconvolve the AGN component from binaries with different origin, we allow for BBH formation in both AGN and phenomenological channels. We consistently find a significant contribution to the merger rate from the AGN

component ($\simeq O(5/\text{Gpc}^{-3}\text{yr}^{-1})$). Our inferred AGN contribution follows by our prior belief on the maximum mass of BBH formed from other channels, which we presume is less than $50M_{\odot}$ due to pair-instability impacts on stellar evolution and death.

As in previous studies (Yang et al. 2020a,b; Gayathri et al. 2020, 2021; Vajpeyi et al. 2022), our models for AGN BBH formation predict a wide range of BBH mass ratios and frequent significant spins. At present, because the distinctive signatures of AGN formation are preferentially imparted only to the most massive BBH, the extant BBH sample does not yet contain enough events to provide overwhelming evidence in favour of an AGN component, consistent with prior work (Vajpeyi et al. 2022) subsequent observations could support or rule out this channel.

Acknowledgements We gratefully acknowledge the support of LIGO and Virgo for the provision of computational resources. G.V. and D.W. acknowledge the support of the National Science Foundation under grant PHY-2207728. I.B. acknowledges the support of the National Science Foundation under grants #1911796, #2110060 and #2207661 and of the Alfred P. Sloan Foundation. This research has made use of data, software and/or web tools obtained from the Gravitational Wave Open Science Center (<https://www.gwopenscience.org>), a service of LIGO Laboratory, the LIGO Scientific Collaboration and the Virgo Collaboration. LIGO is funded by the U.S. National Science Foundation. Virgo is funded by the French Centre National de Recherche Scientifique (CNRS), the Italian Istituto Nazionale della Fisica Nucleare (INFN) and the Dutch Nikhef, with contributions by Polish and Hungarian institutes. This material is based upon work supported by NSF's LIGO Laboratory, which is a major facility fully funded by the National Science Foundation.

REFERENCES

- Aasi, J., et al. 2015, *Class. Quantum Grav.*, 32, 074001, doi: [10.1088/0264-9381/32/7/074001](https://doi.org/10.1088/0264-9381/32/7/074001)
- Abbott, B. P., Abbott, R., Abbott, T. D., et al. 2019, *Phys. Rev. X*, 9, 031040
- Abbott, R., Abbott, T. D., Abraham, S., et al. 2020, arXiv:2010.14533
- Abbott, R., et al. 2021a. <https://arxiv.org/abs/2111.03606>
- . 2021b. <https://arxiv.org/abs/2111.03634>
- . 2021c, *Astrophys. J. Lett.*, 913, L7, doi: [10.3847/2041-8213/abe949](https://doi.org/10.3847/2041-8213/abe949)
- . 2021d. <https://arxiv.org/abs/2108.01045>
- . 2021e, *Astrophys. J. Lett.*, 915, L5, doi: [10.3847/2041-8213/ac082e](https://doi.org/10.3847/2041-8213/ac082e)
- . 2021f, *Phys. Rev. X*, 11, 021053, doi: [10.1103/PhysRevX.11.021053](https://doi.org/10.1103/PhysRevX.11.021053)
- Acernese, F., et al. 2015, *Class. Quantum Grav.*, 32, 024001, doi: [10.1088/0264-9381/32/2/024001](https://doi.org/10.1088/0264-9381/32/2/024001)
- Antonini, F., Murray, N., & Mikkola, S. 2014, *ApJ*, 781, 45, doi: [10.1088/0004-637X/781/1/45](https://doi.org/10.1088/0004-637X/781/1/45)
- Bartos, I., Kocsis, B., Haiman, Z., & Márka, S. 2017, *ApJ*, 835, 165, doi: [10.3847/1538-4357/835/2/165](https://doi.org/10.3847/1538-4357/835/2/165)
- Belczynski, K., Kalogera, V., & Bulik, T. 2002, *ApJ*, 572, 407, doi: [10.1086/340304](https://doi.org/10.1086/340304)
- Carr, B. J., & Hawking, S. W. 1974, *MNRAS*, 168, 399
- de Mink, S. E., & Mandel, I. 2016, *MNRAS*, 460, 3545, doi: [10.1093/mnras/stw1219](https://doi.org/10.1093/mnras/stw1219)

- Delfavero, V., O’Shaughnessy, R., Wysocki, D., & Yelikar, A. 2022, arXiv e-prints, arXiv:2205.14154.
<https://arxiv.org/abs/2205.14154>
- Doctor, Z., Wysocki, D., O’Shaughnessy, R., Holz, D. E., & Farr, B. 2020, ApJ, 893, 35,
 doi: [10.3847/1538-4357/ab7fac](https://doi.org/10.3847/1538-4357/ab7fac)
- Edelman, B., Doctor, Z., Godfrey, J., & Farr, B. 2022, ApJ, 924, 101, doi: [10.3847/1538-4357/ac3667](https://doi.org/10.3847/1538-4357/ac3667)
- Fishbach, M., & Holz, D. E. 2017, Astrophys. J. Lett., 851, L25, doi: [10.3847/2041-8213/aa9bf6](https://doi.org/10.3847/2041-8213/aa9bf6)
- Gayathri, V., Bartos, I., Haiman, Z., et al. 2020, Astrophys. J. Lett., 890, L20, doi: [10.3847/2041-8213/ab745d](https://doi.org/10.3847/2041-8213/ab745d)
- Gayathri, V., Yang, Y., Tagawa, H., Haiman, Z., & Bartos, I. 2021, Astrophys. J. Lett., 920, L42,
 doi: [10.3847/2041-8213/ac2cc1](https://doi.org/10.3847/2041-8213/ac2cc1)
- Gerosa, D., & Fishbach, M. 2021, Nature Astronomy, 5, 749, doi: [10.1038/s41550-021-01398-w](https://doi.org/10.1038/s41550-021-01398-w)
- Kimball, C., Talbot, C., Berry, C. P. L., et al. 2021, ApJL, 915, L35, doi: [10.3847/2041-8213/ac0aef](https://doi.org/10.3847/2041-8213/ac0aef)
- Kimpson, T. O., Spera, M., Mapelli, M., & Ziosi, B. M. 2016, MNRAS, 463, 2443, doi: [10.1093/mnras/stw2085](https://doi.org/10.1093/mnras/stw2085)
- Loredo, T. J. 2004, in American Institute of Physics Conference Series, Vol. 735, Bayesian Inference and Maximum Entropy Methods in Science and Engineering: 24th International Workshop on Bayesian Inference and Maximum Entropy Methods in Science and Engineering, ed. R. Fischer, R. Preuss, & U. V. Toussaint, 195–206,
 doi: [10.1063/1.1835214](https://doi.org/10.1063/1.1835214)
- Mandel, I., Farr, W. M., & Gair, J. R. 2019, MNRAS, 486, 1086, doi: [10.1093/mnras/stz896](https://doi.org/10.1093/mnras/stz896)
- Marchant, P., Langer, N., Podsiadlowski, P., Tauris, T. M., & Moriya, T. J. 2016, A&A, 588, A50,
 doi: [10.1051/0004-6361/201628133](https://doi.org/10.1051/0004-6361/201628133)
- McKernan, B., Ford, K. E. S., Callister, T., et al. 2022, MNRAS, 514, 3886, doi: [10.1093/mnras/stac1570](https://doi.org/10.1093/mnras/stac1570)
- McKernan, B., Ford, K. E. S., Lyra, W., & Perets, H. B. 2012, MNRAS, 425, 460,
 doi: [10.1111/j.1365-2966.2012.21486.x](https://doi.org/10.1111/j.1365-2966.2012.21486.x)
- McKernan, B., Ford, K. E. S., & O’Shaughnessy, R. 2020, MNRAS, 498, 4088, doi: [10.1093/mnras/staa2681](https://doi.org/10.1093/mnras/staa2681)
- McKernan, B., Ford, K. E. S., Bellovary, J., et al. 2018, The Astrophysical Journal, 866, 66,
 doi: [10.3847/1538-4357/aadae5](https://doi.org/10.3847/1538-4357/aadae5)
- Portegies Zwart, S. F., & McMillan, S. L. W. 2000, ApJL, 528, L17, doi: [10.1086/312422](https://doi.org/10.1086/312422)
- Portegies Zwart, S. F., & Yungelson, L. R. 1998, A&A, 332, 173
- Sadiq, J., Dent, T., & Wysocki, D. 2022, PhRvD, 105, 123014, doi: [10.1103/PhysRevD.105.123014](https://doi.org/10.1103/PhysRevD.105.123014)
- Sigurdsson, S., & Hernquist, L. 1993, Nature, 364, 423,
 doi: [10.1038/364423a0](https://doi.org/10.1038/364423a0)
- Stone, N. C., Metzger, B. D., & Haiman, Z. 2017, MNRAS, 464, 946, doi: [10.1093/mnras/stw2260](https://doi.org/10.1093/mnras/stw2260)
- Tagawa, H., Haiman, Z., Bartos, I., & Kocsis, B. 2020a, ApJ, 899, 26, doi: [10.3847/1538-4357/aba2cc](https://doi.org/10.3847/1538-4357/aba2cc)
- Tagawa, H., Haiman, Z., Bartos, I., Kocsis, B., & Omukai, K. 2021, MNRAS, 507, 3362,
 doi: [10.1093/mnras/stab2315](https://doi.org/10.1093/mnras/stab2315)
- Tagawa, H., Haiman, Z., & Kocsis, B. 2020b, ApJ, 898, 25,
 doi: [10.3847/1538-4357/ab9b8c](https://doi.org/10.3847/1538-4357/ab9b8c)
- Talbot, C., & Thrane, E. 2018, ApJ, 856, 173,
 doi: [10.3847/1538-4357/aab34c](https://doi.org/10.3847/1538-4357/aab34c)
- Thrane, E., & Talbot, C. 2019, PASA, 36, e010,
 doi: [10.1017/pasa.2019.2](https://doi.org/10.1017/pasa.2019.2)
- Tiwari, V., & Fairhurst, S. 2021, ApJL, 913, L19,
 doi: [10.3847/2041-8213/abf7e](https://doi.org/10.3847/2041-8213/abf7e)
- Vajpeyi, A., Thrane, E., Smith, R., McKernan, B., & Ford, K. E. S. 2022, The Astrophysical Journal, 931, 82,
 doi: [10.3847/1538-4357/ac6180](https://doi.org/10.3847/1538-4357/ac6180)
- Veske, D., Márka, Z., Sullivan, A. G., et al. 2020, MNRAS, 498, L46, doi: [10.1093/mnras/slaa123](https://doi.org/10.1093/mnras/slaa123)
- Wysocki, D., Lange, J., & O’Shaughnessy, R. 2019, Phys. Rev. D, 100, 043012, doi: [10.1103/PhysRevD.100.043012](https://doi.org/10.1103/PhysRevD.100.043012)
- Yang, Y., Bartos, I., Haiman, Z., et al. 2020a, ApJ, 896, 138
- Yang, Y., Gayathri, V., Bartos, I., et al. 2020b, Astrophys. J. Lett., 901, L34, doi: [10.3847/2041-8213/abb940](https://doi.org/10.3847/2041-8213/abb940)
- Yang, Y., Gayathri, V., Bartos, I., et al. 2020, ApJL, 901, L34, doi: [10.3847/2041-8213/abb940](https://doi.org/10.3847/2041-8213/abb940)
- Zevin, M., Bavera, S. S., Berry, C. P. L., et al. 2021, ApJ, 910, 152, doi: [10.3847/1538-4357/abe40e](https://doi.org/10.3847/1538-4357/abe40e)